Journal of Physics: Conference Series

PAPER • **OPEN ACCESS**

Optical Microscopy as a probe of the rate limiting transport lifetime in $InSb/Al_{1-x}In_xSb$ quantum wells

To cite this article: C J McIndo *et al* 2018 *J. Phys.: Conf. Ser.* **964** 012005

View the article online for updates and enhancements.

Related content

- Electron transport lifetimes in InSb/Al1-xInxSb quantum well 2DEGs
D G Hayes, C P Allford, G V Smith et al.
- Making the most of microscopy
- Development of Tip-Enhanced Near-Field Optical Spectroscopy and Microscopy
Norihiko Hayazawa, Alvarado Tarun, Atsushi Taguchi et al.

This content was downloaded from IP address 148.88.244.142 on 07/03/2018 at 16:44

IOP Conf. Series: Journal of Physics: Conf. Series **964** (2018) 012005 doi:10.1088/1742-6596/964/1/012005

Optical Microscopy as a probe of the rate limiting transport lifetime in InSb/$Al_{1-x}In_xSb$ quantum wells

C J McIndo[1,4], D G Hayes[1], A Papageorgiou[1], L A Hanks [1,5], G V Smith[1], C P Allford[1,2], S Zhang[3], E M Clarke[3] and P D Buckle[1]

[1] School of Physics and Astronomy, Cardiff University, Queen's Buildings, The Parade, Cardiff, CF24 3AA, UK
[2] School of Engineering, University of Warwick, Coventry, CV4 7AL, UK
[3] EPSRC National Centre for III-V Technologies, North Campus University of Sheffield, Sheffield, S3 7HQ, UK

E-mail: mcindocj@cardiff.ac.uk

Abstract. Recent reports of magnetotransport measurements of InSb/$Al_{1-x}In_xSb$ quantum well structures at low temperature (3 K) have shown the need for inclusion of a new scattering mechanism not present in traditional transport lifetime models. Observations and analysis of characteristic surface structures using differential interference contrast DIC (Nomarski) optical imaging have extracted representative average grain feature sizes for this surface structure and shown these features to be the limiting low temperature scattering mechanism. We have subsequently modelled the potential profile of these surface structures using Landauer-Büttiker tunnelling calculations and a combination of a Monte-Carlo simulation and Drude model for mobility. This model matches experimentally measured currents and mobilities at low temperatures, giving a range of possible barrier heights and widths, as well modelling the theoretical trend in mobility with temperature.

1. Introduction

Indium antimonide (InSb) exhibits the lowest reported electron effective mass ($m^* = 0.014\ m_e$) [1] and highest reported room-temperature electron mobility ($\mu = 78{,}000\ cm^2V^{-1}s^{-1}$) [1] of any compound semiconductor. These properties make InSb particularly suited to many electronic applications, including low power high frequency electronics and quantum device realisation. There has been recent interest in the development of high quality InSb material following the report of two-dimensional electron gas (2DEG) channel mobilities in excess of 200,000 $cm^2V^{-1}s^{-1}$ at T = 1.8 K [2-9] and the recent reports of Majorana fermion observation in InSb nanowires [10, 11]. There is renewed interest in this material system, when coupled with superconducting material, to provide a potentially robust quantum system for information processing.

Furthermore, the strong spin-orbit interaction and extremely large Landé g-factor ($g \approx -50$) [1, 12] exhibited in InSb has gained attention for potential exploitation in spintronics and quantum information control [13-15].

[4] Author to whom all correspondence should be addressed
[5] Present address: Physics Department, Lancaster University, Lancaster, LA1 4YB, UK

Content from this work may be used under the terms of the Creative Commons Attribution 3.0 licence. Any further distribution of this work must maintain attribution to the author(s) and the title of the work, journal citation and DOI.
Published under licence by IOP Publishing Ltd

Previous studies of carrier transport in InSb 2DEGs [3, 4] have considered standard scattering mechanisms using the relaxation time approximation, describing the mobility variation over a wide range of temperature (typically 3 K – 300 K). Whilst there has been good agreement, parameters used have tended to be extreme values to enable acceptable fits to data [9]. It has recently been shown that a previously unaccounted for major scattering mechanism due to surface features (hillocks [6-8]), associated with material quality, must be considered, with this having a major effect on the measured mobility. Considering this additional structural scattering allows for more reasonable values for standard scattering mechanisms, showing that there is immense potential for mobility improvement in this material [8]. Due to this potentially large mobility improvement in InSb QWs, there have been further recent investigations into methods of improved MBE growth via buffers and superlattice structures [6], as well as research into hillock growth and formation [7].

2. Growth and Sample Details

Detailed descriptions of the growth and fabrication of samples can be found in references [8] and [9]. In summary, 30 nm InSb quantum well heterostructures were grown by solid source molecular beam epitaxy (MBE) on semi-insulating GaAs substrates (and so are therefore lattice mismatched with regard to the substrate). Hall bar devices with an aspect ratio of 5:1 (nominally 200 μm × 40 μm) were then fabricated using standard techniques for subsequent magnetotransport measurements.

3. Experimental Determination of Mobility and Sheet Carrier Density

We recently reported observed trends in magnetoresistance Hall measurements of several InSb QW samples with the results reproduced here (see references [8] or [9] for experimental details).

Figure 1 shows the extracted mobilities, μ, and carrier densities, n_{2D}, for a range of different samples at 3 K, with samples with increasing δ-doping (filled symbols) broadly defining three regimes in the data. Initially, in region 1, an increasing mobility is observed for an increase in carrier concentration (from 1×10^{11} cm^{-2} to 3×10^{11} cm^{-2}). This is believed to be due to single subband filling, calculated from Schrödinger-Poisson (S.P.) modelling [16], giving rise to increased Thomas-Fermi screening. The mobility then begins to plateau at ~250,000 cm^{2}V^{-1}s^{-1} for a narrow range of carrier densities (region 2), before decreasing beyond 4×10^{11} cm^{-2} (region 3). In region 3, S.P. modelling shows there is the possibility of multiple subband occupancy and additional intersubband scattering.

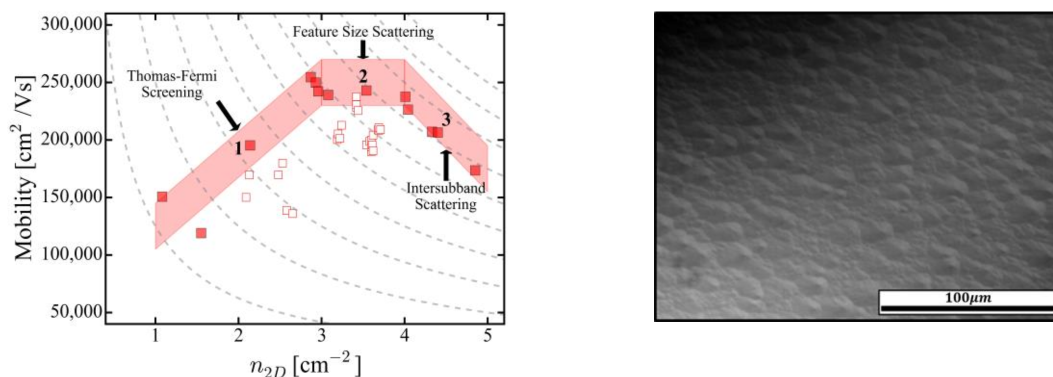

Figure 1. Left: Measured mobility (two carrier fit) vs. 2D sheet carrier density (n_{2D}) from 3 K Hall measurements. A series of samples with increasing δ-doping levels is shown by the larger, filed symbols, broadly defining three regimes (labelled with principal physical cause). Smaller, unfilled symbols indicate similar samples from other growth batches. Dashed lines are contours of constant conductance from 2 mS to 20 mS. Right: Optical Nomarski image of sample surface, magnification × 50, for a sample with n_{2D} ~3×10^{11} cm^{-2} and mobility ~200,000 cm^{2}V^{-1}s^{-1}. The surface is clearly textured, with features of varying sizes.

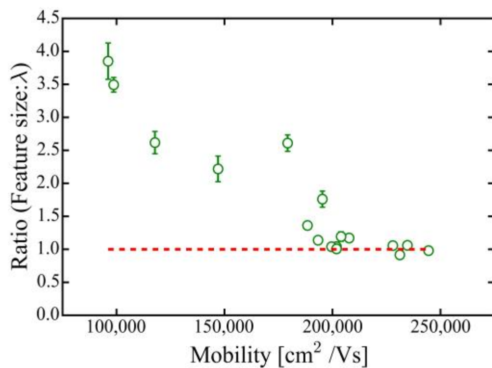

Figure 2. Ratio of mean feature diameter (with one standard deviation error determined from size distributions given by multiple image sampling) to measured mean free patch λ as a function of mobility (open circles), approaching limiting value of 1 (dashed line).

To examine the limiting factors affecting the higher mobility samples, we recently reported on the study of the surface morphology using optical differential interference contrast DIC (Nomarski) imaging [8]. A raw Nomarski image of a standard sample with $n_{2D} \sim 3 \times 10^{11}$ cm^{-2} and $\mu \sim 200{,}000$ cm^{2}V^{-1}s^{-1} is shown in figure 1 at a magnification of × 50.

The Nomarski image shows clear surface roughness, present similarly on all samples imaged [6, 7]. The roughness consists of approximately circular features with clear boundaries separating features. For the samples studied here, the embedded quantum well where the 2DEG resides is situated at a depth of 50 nm below the surface, whereas the threading dislocations that cause these surface features are created at the substrate/buffer interface at a depth of 3 μm. Any dislocations that propagate through the buffer to the quantum well will therefore continue to the surface. Consequently, due to the proximity of the 2DEG to the surface, it is reasonable to assume that this surface roughness, and in particular the boundaries, have a severe impact on the electron transport in the quantum well.

Using basic image analysis techniques (described in reference [8]), we extracted average feature sizes for multiple samples in figure 1. The ratio of the mean feature diameter to the mean free paths, λ, deduced from 3 K Hall mobility data via a basic Drude transport model, is shown in figure 2. Figure 2 shows there is a clear trend in the ratio of feature size with λ, approaching a value of 1 for the highest mobility samples. This limiting value is strongly suggestive that these features, with an average size of ~2.43 ± 0.13 μm, are the low temperature transport lifetime limiting scattering mechanism. At low temperatures, when phonon effects are reduced, an electron traveling in the quantum well may travel ballistically through a feature until it reaches a boundary where it scatters.

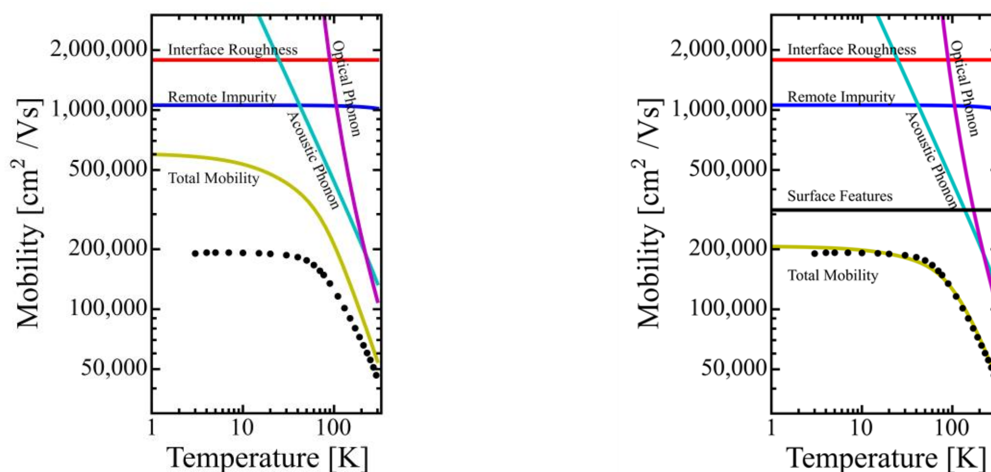

Figure 3. Left: Transport modelled mobility (lines) and measured data (symbols) vs. temperature including standard scattering mechanisms (using typical values [8, 9]). Right: Adapted model including scattering due to 2.43 μm surface features, matching well to Hall measured mobilities.

Transport lifetime modelling of InSb QW devices has been performed previously by Orr *et al* [4] and more recently by McIndo *et al* [8] and Hayes *et al* [9]. These models include several of the standard dominant scattering mechanisms present in III-V heterostructures as well as band non-parabolicity, via a modified effective mass, deduced from a six-band Kane model [3, 17, 18].

By consideration for parameters for each sample, including n_{2D} at 3 K, and reasonable values of background p-type impurities (~1 – 10 × 10^{15} cm^{-3}) it was shown [8, 9] that the mobility could not be matched to measured data without the inclusion of surface feature scattering derived from a Drude model, given by

$$\frac{1}{\tau_l} = \left(\frac{h}{m^*\sqrt{2\pi}}\right)\left(\frac{l_e}{\sqrt{n_{2D}}}\right)^{-1} \quad (1)$$

where l_e is the mean feature size, assuming inelastic scattering occurring at the boundaries. The background impurity density has subsequently been experimentally measured at ~2 × 10^{13} cm^{-3} through low temperature Hall measurements on AlInSb flat layers. A typical graph of the modelled temperature dependant mobility, including a non-parabolic effective mass, is shown in figure 3 left, excluding surface feature scattering. Figure 3 right is modified to include surface feature scattering following equation (1). As can be seen, the model matches well the measured data for a sample with a 3 K mobility of approximately 200,000 cm^{2}V^{-1}s^{-1}. In the low temperature regime the dominant scattering mechanism is associated with the surface features, whereas at high temperature, the mobility is dominated by phonon scattering processes.

4. Modelling of surface feature potential profile

In the transport model above, it was assumed that surface features are regions of constant potential where transport occurs ballistically, whereas the boundaries between features act as potential barriers (scattering centres). These features are believed to be caused by screw-like growth around a threading dislocation [7], with the barriers at the boundaries due to the nonconformity in the crystal structure, giving rise to effective barrier widths of several monolayers. Landauer-Büttiker theory has been used to calculate tunnelling currents, and a combination of a Monte-Carlo (MC) simulation and a simple Drude model has been used to calculate corresponding mobilities. The measured and calculated parameters for the sample modelled are given in table 1, where the number of barriers is given by the length of the Hall bar divided by the average feature size. The width of the barriers is assumed negligible compared to the spacing between barriers.

Table 1. Measured and calculated parameters of sample modelled.

Parameter	Symbol	Value	Parameter	Symbol	Value
Number of barriers	N	82	Experimental current	I	1 μA
Carrier density	n_{2D}	3 × 10^{11} cm^{-2}	Experimntal voltage	V	0.4 mV
Limiting mobility	μ	270,000 cm^{2}V^{-1}s^{-1}	Mean feature size	l_e	2.43 μm

Following references [18] and [19], a tunneling current density, J, can be obtained for a confined 2D sheet of charge (xy) tunneling through barriers in the y direction for an applied voltage, V,

$$J = \frac{2e}{h}\int_0^\infty \left[n_{1D}(E_F - E_y) - n_{1D}(E_F - E_y - eV)\right]T(E_y)\mathrm{d}E_y \quad (2)$$

$$n_{1D}(E_F) = \frac{\sqrt{2m^*}}{h}\int_0^\infty \left(\sqrt{E_x}\right)^{-1}\left[1 + \exp\left((E_x - E_F)/k_B T\right)\right]^{-1}\mathrm{d}E_x \quad (3)$$

where E_F is the Fermi energy (calculated from n_{2D}, accounting for non-parabolic effects using a six band Kane model [3, 17, 18]), T is the temperature, k_B is the Boltzmann constant and $T(E_y)$ is the energy dependent transmission coefficient. For a specific barrier height, width and applied voltage, $T(E_y)$ can be obtained numerically following Tsu and Esaki [19] or Ando and Itoh [20]. Once the Monte Carlo simulation is performed, an effective $T^*(E_y)$ for N barriers can be calculated using the simulation results, however this is expected to be approximately equal to $T(E_y)$.

Barrier heights were determined for barriers from 1 to 50 monolayers (MLs) by calculating $T(E_y)$ and J and matching this to the values in table 1. Barrier heights (in eV) were found to approximately follow the form: height $\approx$ width$^{-1.25} \times 9.41$, where width is measured in MLs. Subsequently, the MC simulation was run to determine a corresponding mobility. For the MC model it is assumed [21] that the left contact is a perfect source/emitter/reflector and the right contact is a perfect sink/acceptor. The electrons are non-interacting and travel at a constant velocity, v, between barriers, determined by their energy. As applied voltage is small compared to barrier heights, this is neglected. Each barrier is identical and separated by the mean feature size, l_e. If a particle is transmitted, no collision occurs, whereas a refection is a scattering event. The mobility can then be calculated as an average over particles by using a simple Drude model,

$$\mu = \frac{e\tau}{m^*} = \frac{e}{m^*}\overline{\left(\frac{t}{N_c}\right)} = \frac{e}{m^*}\frac{l_e}{v} \times \overline{\left(\frac{N_s}{N_c}\right)} \tag{4}$$

where τ is the average time between collisions, t the total time taken for a particle to travel from contact to contact, N_c is the corresponding number of collisions and N_s is the number of steps taken. At finite temperatures, conduction occurs over a spread of energies proportional to the rate of change of the Fermi distribution, f, and so an energy average of mobility must be performed, accounting for a temperature dependent band gap, Fermi energy and effective mass at each energy [22].

The resultant mobilities for barriers from 1 to 50 MLs are shown in figure 4. This is a replot of figure 3, replacing the surface feature scattering given by equation (1) with that from the MC model, and as before, the total mobility closely matches that experimentally measured. The inset shows $T^*(E_y)$ at 3 K (solid lines) and Fermi distributions as a function of energy for 3 K and 300 K (dashed). The colour of the surface feature scattering and of $T^*(E_y)$ represents the barrier width in monolayers.

Figure 4 clearly shows the low temperature mobility is consistent for all barrier widths (due to the approximately constant value of $T^*(E_y)$ at $E = E_F$). At higher temperatures the mobility trends for each barrier width begin to diverge (due to the relation between $T^*(E_y)$ and the Fermi distribution), however the different barrier shapes dependencies' do not diverge until T is greater than ~70 K. At this temperature, transport modelling shows phonon scattering is dominant, and it is therefore not possible to precisely determine the shape of potential barrier due to surface features on this sample.

These figures do show however that the low temperature limiting scattering due to surface features can be modelled as a series of potential barriers, with a range of widths, matching measured currents and Hall mobilities to those calculated through tunneling currents and Monte Carlo simulations. It can also be seen from the figure that above 50 ML the surface feature mobility begins to grow exponentially at higher temperatures. It is reasonable therefore that barrier thicknesses must be smaller than 50 ML, consistent with the possible cause of screw-like growth around a threading dislocation, with micro twin defects at the boundaries.

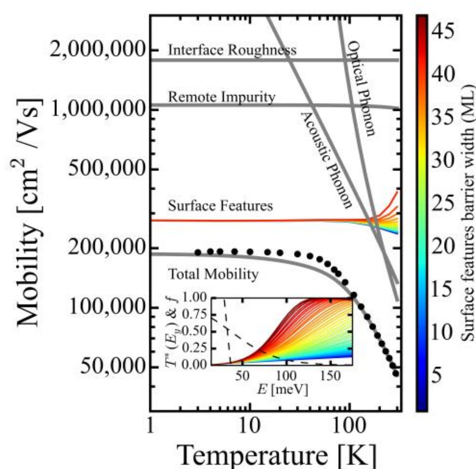

Figure 4. Reproduction of figure 3 with the MC modelled mobility due to scattering from surface features for 1 ML (bottom) to 50 ML (top) width barriers. Inset: Transmission $T^*(E_y)$ at 3 K vs energy (solid lines) for barriers from 1 ML (bottom) to 50 ML (top) as well as Fermi distribution f vs energy for 3 K and 300 K. For surface feature scattering and $T^*(E_y)$, colours represent barrier widths (see online for colour version of figure).

5. Conclusions

We have studied InSb/AlInSb QW 2DEG material and have shown evidence for three characteristic regimes in the measured low temperature Hall mobility behaviour with carrier density. We have demonstrated the application of image analysis techniques to extract representative feature sizes and through use of a transport lifetime model, shown these to be the dominant low temperature mobility limiting scattering mechanism. We have subsequently used Monte-Carlo simulations to model the current, and the limiting mobility due to these features. Through use of a combination of Landauer-Büttiker and Drude models, we have demonstrated the possible range of potential barrier heights and widths, from 1 ML to 50 ML, and shown these to be consistent with scattering corresponding to surface features as the dominant scattering mechanism. This work shows that with correct buffer redesign there is a clear potential for significant improvement in the mobility of such material.

Acknowledgements

The work was supported by the UK Engineering and Physical Sciences Research Council [grant numbers EP/L012995/1 and EP/M507842]. Data supporting this research is openly available from the Cardiff University Research Portal at http://dx.doi.org/10.17035/d.2017.0040827720.

References

[1] Madelung O, Rössler U and Schulz M 2002 *Landolt and Bornstein - Group III Condensed matter: Group IV Elements, (IV-IV) and (III-V) Compounds. Part b - Electronic, Transport, Optical and Other Properties* (Berlin: Springer).
[2] Yi W *et al* 2015 *Appl. Phys. Lett.* **106** 142103
[3] Pooley O J, Gilbertson A M, Buckle P D, Hall R S, Emeny M T, Fearn M, Halsall M P, Cohen L F and Ashley T 2010 *Semicond. Sci. Technol.* **25** 125005
[4] Orr J M S, Gilbertson A M, Fearn M, Croad O W, Storey C J, Buckle L, Emeny M T, Buckle P D and Ashley T 2008 *Phys. Rev.* B **77** 165334
[5] Qu F *et al* 2016 *Nano Lett.* **16** 7509-13
[6] Zhao X, Zhang Y, Guan M, Cui L, Wang B, Zhu Z and Zeng Y 2017 *J. Cryst. Growth* **470** 1-7
[7] Shi Y, Gosselink D, Gharavi K, Baugh J and Wasilewski Z R 2017 *J. Cryst. Growth* (*Preprint*)
[8] McIndo C J, Hayes D G, Papageorgiou, Hanks L A, Smith G V, Allford C P, Zhang S, Clarke E M and Buckle P D 2017 *Physica* E **91** 169–72
[9] Hayes D G, Allford C P, Smith G V, McIndo C, Hanks A L, Gilbertson A M, Cohen L F, Zhang S, Clarke E M and Buckle P D 2017 *Semicond. Sci. Technol.* **32** 085002
[10] Mourik V, Zuo K, Frolov S M, Plissard S R, Bakkers E P and Kouwenhoven L P 2012 *Science* **336** 1003–7
[11] Deng M T, Yu C L, Huang G Y, Larsson M, Caroff P and Xu H Q 2012 *Nano Lett.* **12** 6414–9
[12] Nedniyom B Nicholas R J, Emeny M T, Buckle L, Gilbertson A M, Buckle P D and Ashley T 2009 *Phys. Rev.* B **80** 125328
[13] van den Berg J W G, Nadj-Perge S, Pribiag V S, Plissard S R, Bakkers E P A M, Frolov S M and Kouwenhoven L P 2013 *Phys. Rev. Lett.* **110** 066806
[14] Li R, You J Q, Sun C P and Nori F 2013 *Phys. Rev. Lett.* **111** 086805
[15] Awschalom D D, Basset L C, Dzurak A S, Hu E L and Petta J R 2013 *Science* **339** 1174–9
[16] Tan I-H, Snider G L, Chang L D and Hu E L 1990 *J. Appl. Phys.* **68** 4071
[17] Gilbertson A M, Branford W R, Fearn M, Buckle L, Buckle P D, Ashley T and Cohen L F 2009 *Phys. Rev.* B **79** 235333
[18] Davies J H 1998 *The Physics of Low-Dimensional Semiconductors: An Introduction* (Cambridge: Cambridge University Press)
[19] Tsu R and Esaki L 1973 *Appl. Phys. Lett.* **22** 562
[20] Ando Y and Itoh T 1987 *J. Appl. Phys.* **61** 1497
[21] Bagwell P F and Orando T P 1989 *Phys. Rev*. B **40** 1456
[22] Asgari A and Faraone L 2011 *J. Appl. Phys.* **110** 113713